Rapid Communications

Observation of Fourier transform limited lines in hexagonal boron nitride

A. Dietrich,[1] M. Bürk,[1] E. S. Steiger,[1] L. Antoniuk,[1] T. T. Tran,[2] M. Nguyen,[2] I. Aharonovich,[2] F. Jelezko,[1,3] and A. Kubanek[1,3]

[1]*Institute for Quantum Optics, Ulm University, D-89081 Ulm, Germany*

[2]*Institute of Biomedical Materials and Devices, Faculty of Science, University of Technology Sydney, Ultimo, New South Wales 2007, Australia*

[3]*Center for Integrated Quantum Science and Technology (IQst), Ulm University, D-89081 Ulm, Germany*

(Received 20 December 2017; published 31 August 2018)

Single defect centers in layered hexagonal boron nitride are promising candidates as single-photon sources for quantum optics and nanophotonics applications. However, spectral instability hinders many applications. Here, we perform resonant excitation measurements and observe Fourier transform limited linewidths down to ≈50 MHz. We investigated the optical properties of more than 600 single-photon emitters (SPEs) in hBN. The SPEs exhibit narrow zero-phonon lines distributed over a spectral range from 580 to 800 nm and with dipolelike emission with a high polarization contrast. Finally, the emitters withstand transfer to a foreign photonic platform, namely, a silver mirror, which makes them compatible with photonic devices such as optical resonators and paves the way to quantum photonics applications.

DOI: 10.1103/PhysRevB.98.081414

Single-photon emitters (SPEs) are prime building blocks for a variety of applications in integrated quantum photonics, quantum information processing, and fundamental studies of quantum optics [1–6]. The availability of Fourier transform (FT) limited photons, without spectral diffusion, dephasing, or competing phonon processes, is required for the majority of these applications [1–6]. Single-photon sources with FT limited lines have been demonstrated with atoms or ions in gas-phase organic materials, as well as with solid state systems such as quantum dots and color centers in diamond [7,8]. While those systems have been explored in some of the pioneering nanophotonic experiments, a bright, robust FT limited source that is easily accessible remains a challenge.

In this regard, a new emerging class of SPEs is embedded in two-dimensional host materials such as hexagonal boron nitride (hBN) that offers high brightness and may enable novel architectures for integrated quantum technologies [9,10]. The optical properties are promising with a high photostability [11], high brightness [12–14], a large Debye-Waller factor [15,16], good polarization contrast [17–19], spectral tunability [14,15], stable optical lines as narrow as 45 μeV at cryogenic temperatures [16,20], and, very recently, resonant excitation with lines measured in photoluminescence excitation (PLE) as narrow as 1 GHz [21]. However, the close proximity of the SPE to the host surface makes it susceptible to spectral instability, typically exhibiting a blinking, rapid spectral diffusion and pure dephasing rates much larger than the population decay rates, and therefore zero-phonon lines (ZPLs) much broader than the natural linewidth [22].

In this Rapid Communication, we demonstrate spectrally stable, single-photon emission from the defect center in hBN under resonant excitation without significant spectral diffusion for as long as 30 s. We performed a detailed study of 627 different defect centers in hBN with a central emission wavelength from 580 to 800 nm [17,18,21,23–25]. Resonant excitation reveals linewidths within the FT limit of approximately 55 ± 10 MHz. Our investigated platform consists of two-dimensional hBN flakes mounted on a silver mirror which enables direct integration into photonic structures such as optical resonators, for example, for spin-photon interfaces with Purcell-enhanced, lifetime-limited, single-photon emission.

The hBN flakes are cooled in a continuous-flow cryostat to liquid-helium temperature [see Fig. 1(a)]. The excitation and emission polarization is extracted by a linear polarizer and a λ-half-wave plate probing the incident or emitted polarization via a spectrometer and/or via Avalanch PhotoDiode (APD) counts. For resonant excitation we use a cw Matisse DS dye laser system, which has a mode hop-free scanning range of $>$40 GHz and a linewidth of $<$250 kHz. The wavelength of the laser is monitored via a wave meter from High Finesse with 500-kHz resolution and an acquisition frequency up to 600 Hz. Photoluminescence excitation (PLE) is measured by detecting the phonon-sideband (PSB) emission while the direct laser light is blocked with a low-pass (LP) filter.

We evaluate emission spectra from many different SPEs and measure the second-order autocorrelation function in a Hanbury-Brown and Twiss setup (HBT) with $g^2(\tau = 0) < 0.5$, proving the single-photon character of the SPE [see Fig. 1(c)]. The data fit is based on the $g^2(\tau)$ model for a two-level system,

$$g^2(\tau) = 1 - ae^{|\tau|/\tau_0}. \quad (1)$$

Various sites have lifetimes in the range of $\tau_0 \approx 1.53$–2.88 ns, resulting in a natural linewidth of $\Gamma \approx 55$–84 MHz, in agreement with previous results [15,21,22]. A background signal originating from the fluorescence of the silver mirror under off-resonant excitation leads to a signal-to-noise ratio of ≈1.4. Background subtraction results in $g^2(\tau) = 0.01$.

As described in Ref. [26], linear polarized or circular polarized dipoles are expected from a symmetry-based group theory approach of the defect centers. We prove the polarization properties by measuring the emission polarization (red data) for the emitter at a 602-nm emission wavelength in Fig. 1(d), with a contrast as high as 0.9 and with an average of 0.6 from

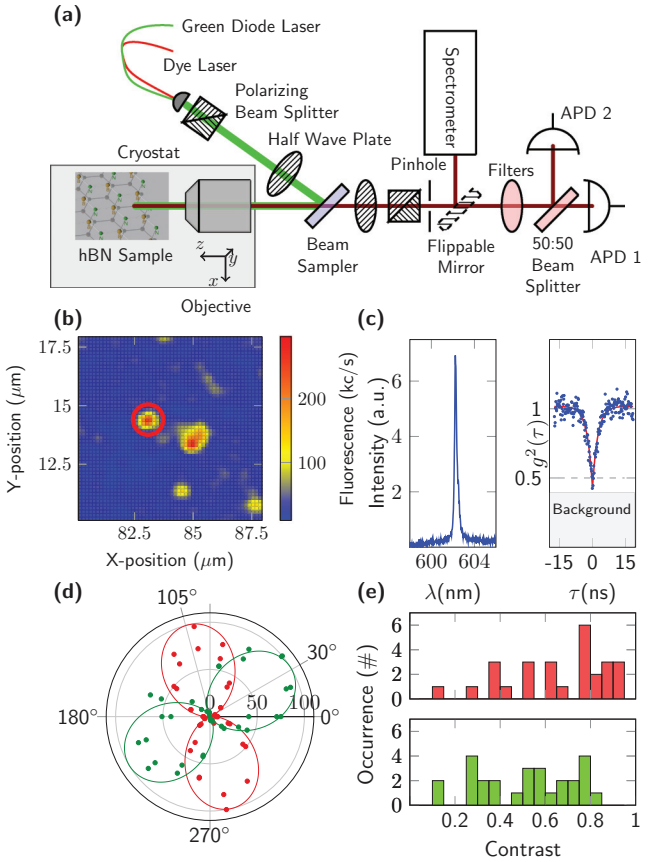

FIG. 1. (a) Experimental setup. The hBN sample is cooled to a liquid-helium temperatures of ≈5 K in a continuous flow cryostat and investigated via a custom-built confocal microscope with a high numerical aperture (NA) objective of 0.9. All PL and polarization measurements are performed under identical conditions, in off-resonant excitation with a 532-nm green diode laser and with a power of up to 250 μW in front of the objective. A spectrometer with an maximal resolution of 16 GHz records the PL spectra with a acquisition time of 10 s and an HBT setup enables one to extract second-order photon correlations. For polarization measurements we use an additional polarizer and a λ -half-wave plate. Resonant excitation was performed using a cw Matisse DS dye laser. (b) Confocal scan (maximum 200×200 μm) of the emitters in hBN flakes with off-resonant excitation. (c) Off-resonant spectrum and second-order correlation of the emitter marked in (b). $g^2(0) = 0.42$ reveals the single-photon character of the SPE. Background subtraction, originating from a signal-to-noise ratio of ≈1.4, results in $g^2(0) = 0.01$. The lifetime is then extrapolated to 2.37 ± 0.12 ns corresponding to a natural linewidth of $\approx 67.2 \pm 3.2$ MHz. (d) and (e) We find emission and excitation are misaligned by 75°. The polarization contrast of emission (red data) has an average 0.6 and for excitation (green data) 0.5.

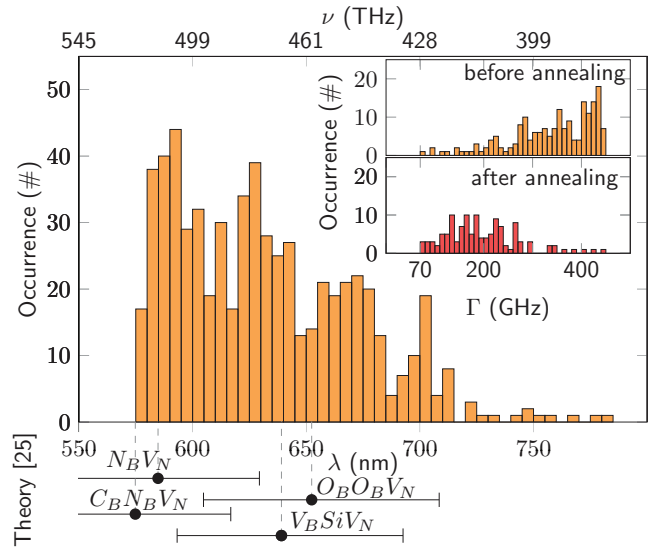

FIG. 2. Histogram of 627 individual ZPLs binned within a 10-nm cluster around four emission wavelengths at 590, 630, 670, and 700 nm. Another cluster is indicated at 750 nm. We compare this distribution to density functional theory (DFT) calculated ZPL energies of the color center with an error margin of 0.3 eV [25]. Inset: Histogram of 627 off-resonantly excited (see Fig. 1) emitter linewidths before (yellow bars) and 121 linewidths after annealing (red bars) in vacuum at 500 °C for 1 h. The average linewidth decreases by about 120 GHz.

the statistics of the 28 emitters in the data shown in red in Fig. 1(e). The contrast is defined as

$$C = \frac{I_{\max} - I_{\min}}{I_{\max} + I_{\min}}. \quad (2)$$

Deviation from perfect polarization contrast may originate from a nonperfect horizontal alignment of the hBN flakes with respect to the substrate. We infer the polarization dependence for the off-resonant excitation by placing the polarizer in the excitation path and recording the fluorescence depending on the excitation angle [see Fig. 1(a)]. The polarization in off-resonant excitation results in a significantly reduced contrast of on average 0.5, reflecting the incoherent process and indicating that polarization is not preserved in phonon-assisted excitation.

PL spectra are recorded for 627 individual ZPL lines, distributed from 580 to 800 nm [see Fig. 2(a)]. The ZPL emission frequencies cluster in four distinct positions, with peaks at 590, 630, 670, and 700 nm with an overall decreasing occurrence with increasing wavelength. Another cluster is indicated at 750 nm. Each cluster could originate from a specific emitter composition with an inhomogeneous spectral linewidth of about full width at half maximum (FWHM) ≈ 25 nm [27]. In-depth knowledge of the SPE formation could be gained by a comparison with *ab initio* calculations as developed in Refs. [25,28]. The grouping into four distinct regions can be correlated to the simulated compositions of the defects as depicted on the bottom of Fig. 2. The high-energy emission is likely to correlate to the neutrally charged $N_B V_N$ defect [25,28]. The lower-energy emission is likely to correlate to the proposed carbon-related defects, the positively charged $(V_N C_B)$ [26] and the $C_N V_B$ defect [25]. While our work is beyond the scope of concretely isolating the selected defect, we note that these defects have a similar crystallographic symmetry and therefore are expected to yield a similar resonant excitation behavior. Our data could be used to refine and calibrate future *ab initio* calculations. The observed spectral diffusion is in accord with the calculated structure that suggests a persistent dipole moment.

In the inset of Fig. 2 we plot the histogram of the SPE linewidths, before and after an additional annealing at 500 °C

for 1 h. Before annealing, the average linewidth of the 612 individual sites is 339 GHz, while after annealing the linewidth reduces to 213 GHz (see the inset of Fig. 2). All measurements were recorded under 250 μW of 532-nm excitation, using a spectrometer resolution of 16 GHz and 10-s acquisition time. The improved linewidth can be explained by the elimination of chemical residue on the surface, which also improves the broad background fluorescence as reported in Ref. [29]. However, in both cases the narrowest observed linewidth of ≈70 GHz is still limited by significant spectral diffusion, which could arise from charge fluctuations on the surface [30,31].

Resonant excitation further reduces the linewidth with respect to off-resonant excitation. We investigate the resonant excitation of a SPE with an emission line at 713 nm, which showed a narrow inhomogeneous linewidth of 293 GHz [see Fig. 3(a)], and which is well suited for our resonant excitation dye laser. The emission spectrum indicates a second emitter at ≈755-nm emission wavelength as well as phonon-assisted emission at 785 nm that we use for the detection during resonant excitation, while blocking the laser with a 750-nm LP filter. To separate the PSB emission from our emitter at 713 nm from fluorescence originating from the additional emitter at 755 nm, we record the spectrum in off-resonant excitation [blue spectra, inset of Fig. 3(a)], as well as in resonant excitation [red spectra, inset of Fig. 3(a)]. Due to resonant excitation, the background signal, which is partially caused from excitation of another SPE and fluorescence of the silver mirror under off-resonant excitation, vanished, so the PSB of the emitter can be seen. The recorded phonon peak at around 785 nm corresponds to a phonon mode of hBN at 187 meV (45 THz or 1500 cm^{-1}) as reported in Refs. [32–35]. According to Ref. [37], this mode is assigned to be a longitudinal optic mode with a group symmetry of E_{1u}. Detecting phonon-assisted fluorescence from this mode while resonantly exciting the SPE enables us to perform PLE spectroscopy [38].

Resonant excitation reveals blinking in the fluorescence signal as shown in Fig. 3(b), with an "OFF" state corresponding to a background level of 300 counts/s, a clear "ON" state corresponding to 3000 ± 500 counts/s, and no visible photobleaching. Eventually very long periods of stable fluorescence occur for many seconds which we attribute to slowly fluctuating, trapped carrier-induced Stark shifts, followed by large spectral jumps as reported in Ref. [39]. Such periods of stable fluorescence enable us to perform resonant confocal scans without any significant change in the fluorescence signal [see the inset of Fig. 3(c)]. Detailed time-resolved statistics of the blinking timescale is unfolded by a histogram of the ON times over their occurrence with a binning of 0.2 s in Fig. 3(c). A fit with an exponential decay reveals a single time constant of $\tau = 0.378 \pm 0.017$ s.

In order to record the linewidth in resonant excitation we perform PLE line scans faster than the characteristic diffusion time $\tau = 0.378$ s. The slowest applied scanning speed of the resonant laser is about 133 MHz/s with a recording frequency of 50 Hz. We obtained the best signal-to-noise ratio for 4–6 μW excitation power in front of the objective, while we made sure to be well below saturation.

Several PLE scans performed over a range of 200 GHz of the same SPE emitting at 713 nm uncover the histogram

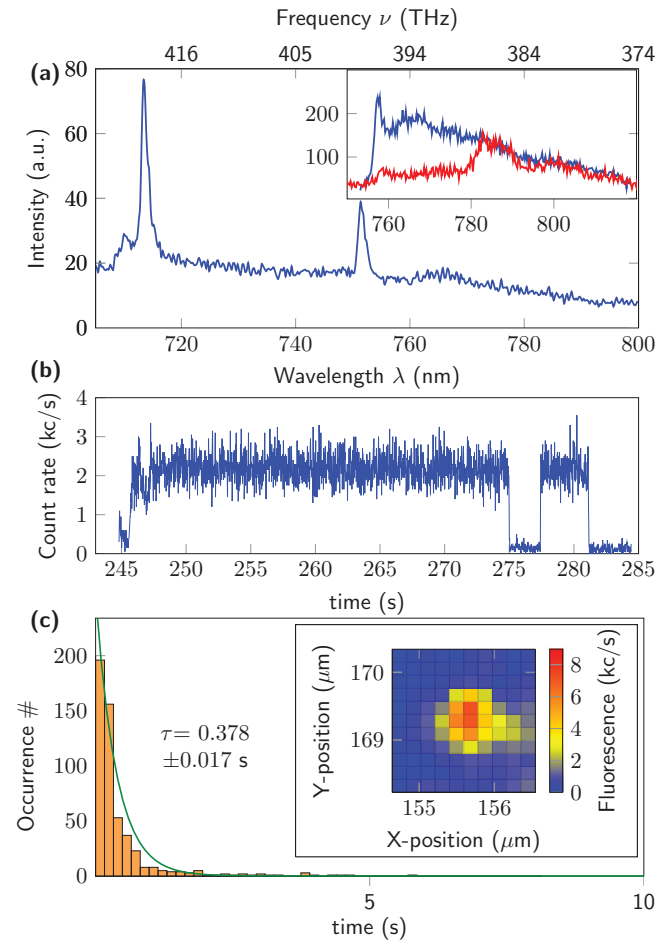

FIG. 3. (a) PL spectrum of the investigated emitter at an emission wavelength of 713 nm with an additional emitter at 755 nm, acquired with parameters given in Fig. 1(a). Inset: The sideband is measured with a 750-nm LP filter with off-resonant (blue data) and resonant (red data) excitation. Resonant excitation separates the phonon sideband of the 713-nm emitter from the additional emitter at 755 nm. The phonon mode at 785 nm with 185 meV (45 THz, 1500 cm^{-1}) matches the reported local longitudinal optic (LO) mode of hBN [32–35]. (b) The fluorescence time trace is stable under resonant excitation for as long as 30 s. (c) Statistics of the ON time of the fluorescence traces discloses a time constant of 0.37 s for spectral instabilities. Inset: Spectral stability is long enough to extract two-dimensional maps of the emitter in resonant excitation without significant fluctuations of the fluorescence signal.

displayed in Fig. 4(a). Scans beyond this 200 GHz revealed no signal. We normalize the statistics of occurrences in Fig. 4(a) (right axis), taking into account the number of scans per bin (6 GHz). The normalized PLE statistic discloses a spectral width of ≈67.5 ± 9.5 GHz, much narrower than the inhomogeneous PL linewidth of ≈293.39 ± 8.13 GHz [blue data and Gaussian fit in Fig. 4(a)]. We filtered out all data which showed blinking during laser scanning. Ongoing blinking and diffusion dynamics hinder further investigations on the fine structure, necessitating additional surface treatment and passivation techniques. The lifetime of this line is ≈2.88 ns, giving a FT limited linewidth of $\Gamma_{\text{nat}} = 55.26 \pm 0.19$ MHz. While

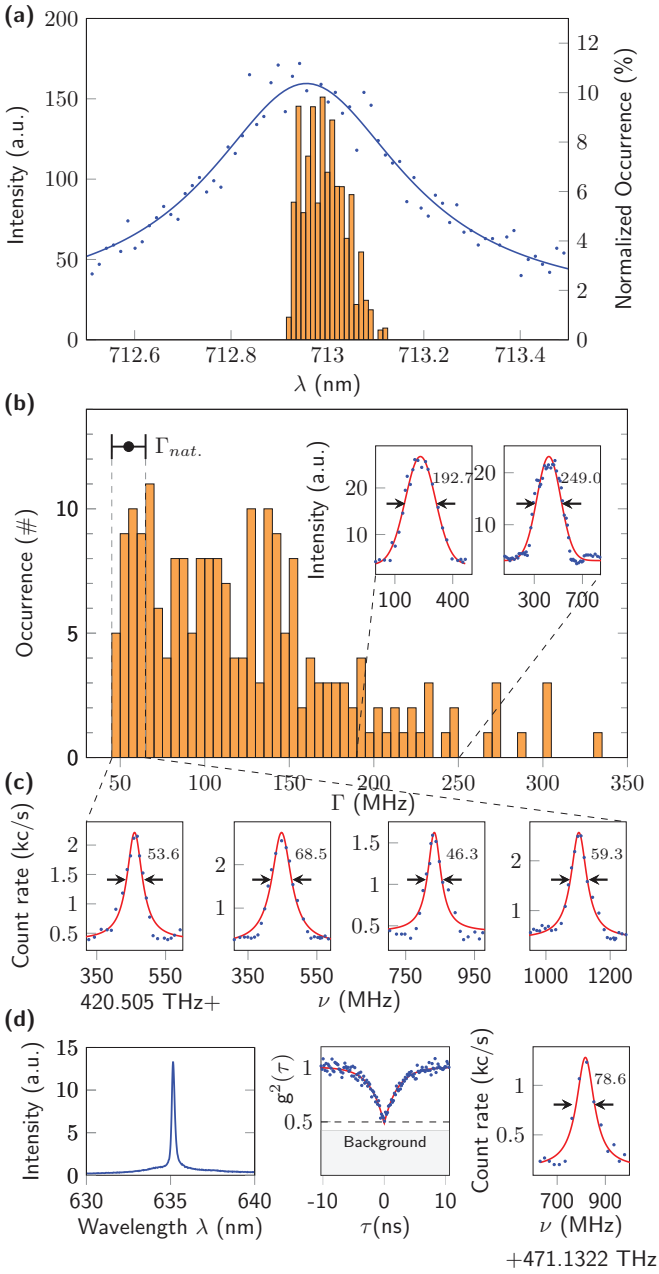

FIG. 4. (a) The PL spectrum (blue data) has an inhomogeneous linewidth of $\approx 293.39 \pm 8.13$ GHz. The histogram of 204 PLE lines measured for the same emitter over a range of 200 GHz reveals an inhomogeneous linewidth of $\approx 67.5 \pm 9.5$ GHz. (b) The homogeneous linewidth extracted from more than 204 PLE line scans of the same emitter unfolds 124.5 ± 60.5 MHz. The large variance hints at ongoing dynamics on the second timescale of the performed scans. (c) About 39 lines of that specific emitter are fitted with a Lorentzian line shape and lie within an error margin of the natural linewidth of 55 ± 10 MHz. For details on the evaluation, see the Supplemental Material [36]. (d) We reproduced FT limited lines on a second emitter with an emission wavelength at 635 nm with a natural linewidth of $\Gamma_{\text{nat}} = (60.1 \pm 3.4)$ MHz inferred from a second-order correlation function and a time constant of 0.015 s.

the homogeneous linewidth of 124.5 MHz is still more than twice as large as the FT limited linewidth, the large variance of 60.5 MHz after averaging over all 204 lines indicates ongoing dynamics on the timescale of the resonant laser scan. Details of the linewidth statistic in Fig. 4(b) show a vast spread with a linewidth up to 200 MHz. Two examples of the broadened resonant lines are shown in the inset. Note that these lines are fit well with the Gaussian function. We suspect that the diffusion dynamics discussed above causes this spectral broadening. Nevertheless, about 39 lines out of all 204 lines are within the error margin of 10 MHz of the natural linewidth. We fitted the lines with a Lorentz function and four example lines are shown in Fig. 4(c), displaying FT limited lines with a linewidth of 46–60 ± 10 MHz. The uncertainty of 10 MHz arises from the systematic error of the measurement and the evaluation algorithm. We manifest the FT limited line with a second SPE that exhibits a ZPL at 635 nm [Fig. 4(d)]. A second-order autocorrelation measurement extracted to zero excitation power [40] with a similar background yields a natural linewidth of $\tau_{\text{nat}} = (60.1 \pm 3.4)$ MHz (see Supplemental Material [36]). This natural linewidth can be compared with the PLE measured linewidth of (78.6 ± 1.3) MHz [see Fig. 4(d)].

In summary, we have demonstrated FT limited, single-photon emission from two different defect centers in hBN without significant spectral diffusion or spectral instability for as long as 30 s. A conservative extrapolation from the reported count rates of ≈2000 counts/s, measured well below saturation and detecting only a small fraction of the sideband emission, yields indistinguishable single-photon emission rates much larger than 20 000 counts/s in the current setting, assuming a Debye-Waller factor of 0.82 as reported in Ref. [12].

The investigated platform consists of hBN flakes placed on a silver mirror and opens a different perspective for resonance fluorescence experiments or investigations of mirror image interactions. The architecture demonstrates the compatibility with photonic platforms, in particular, optical resonators, for Purcell-enhanced single-photon emission facilitating indistinguishable photon rates up to GHz rates. Some SPE in hBN could potentially inhere long spin coherence time [28,41]. In addition, our detailed investigations of more than 627 SPEs in hBN give input for theoretical predictions of the composition of the defects by comparing *ab initio* simulations [26] with the reported emission frequencies.

A.K. and A.D. acknowledge S. Häußler and M.Metsch for fruitful discussions and experimental support. A.K. acknowledges the generous support of the DFG, the Carl-Zeiss Foundation, IQST, and the Wissenschaflter-Rückkehrprogramm GSO/GZS. F.J. acknowledges support of the DFG (Grant No. INST40/502-1), BMBF, VW Stiftung, and EU (ERC, DIADEMS). I.A. acknowledges the generous support of the Alexander van Humboldt Foundation, and the Asian Office of Aerospace Research & Development (Grant No. FA2386-17-1-4064), the Office of Naval Research Global (Grant No. N62909-18-1-2025), and the Australian Research Council (DP180100077). Experiments performed for this work were operated using the Qudi software suite [42].

[1] D. L. Moehring, P. Maunz, S. Olmschenk, K. C. Younge, D. N. Matsukevich, L.-M. Duan, and C. Monroe, Nature (London) **449**, 68 (2007).

[2] S. Ritter, C. Nölleke, C. Hahn, A. Reiserer, A. Neuzner, M. Uphoff, M. Mücke, E. Figueroa, J. Bochmann, and G. Rempe, Nature (London) **484**, 195 (2012).

[3] H. Bernien, B. Hensen, W. Pfaff, G. Koolstra, M. S. Blok, L. Robledo, T. H. Taminiau, M. Markham, D. J. Twitchen, L. Childress, and R. Hanson, Nature (London) **497**, 86 (2013).

[4] T. Legero, T. Wilk, M. Hennrich, G. Rempe, and A. Kuhn, Phys. Rev. Lett. **93**, 070503 (2004).

[5] R. Lettow, Y. L. A. Rezus, A. Renn, G. Zumofen, E. Ikonen, S. Götzinger, and V. Sandoghdar, Phys. Rev. Lett. **104**, 123605 (2010).

[6] A. Sipahigil, M. L. Goldman, E. Togan, Y. Chu, M. Markham, D. J. Twitchen, A. S. Zibrov, A. Kubanek, and M. D. Lukin, Phys. Rev. Lett. **108**, 143601 (2012).

[7] B. Lounis and M. Orrit, Rep. Prog. Phys. **68**, 1129 (2005).

[8] P. Senellart, G. Solomon, and A. White, Nat. Nanotechnol. **12**, 1026 (2017).

[9] A. W. Schell, H. Takashima, T. T. Tran, I. Aharonovich, and S. Takeuchi, ACS Photonics **4**, 761 (2017).

[10] T. T. Tran, D. Wang, Z.-Q. Xu, A. Yang, M. Toth, T. W. Odom, and I. Aharonovich, Nano Lett. **17**, 2634 (2017).

[11] M. Kianinia, B. Regan, S. A. Tawfik, T. T. Tran, M. J. Ford, I. Aharonovich, and M. Toth, ACS Photonics **4**, 768 (2017).

[12] T. T. Tran, K. Bray, M. J. Ford, M. Toth, and I. Aharonovich, Nat. Nanotechnol. **11**, 37 (2016).

[13] L. J. Martínez, T. Pelini, V. Waselowski, J. R. Maze, B. Gil, G. Cassabois, and V. Jacques, Phys. Rev. B **94**, 121405(R) (2016).

[14] G. Grosso, H. Moon, B. Lienhard, S. Ali, D. K. Efetov, M. M. Furchi, P. Jarillo-Herrero, M. J. Ford, I. Aharonovich, and D. Englund, Nat. Commun. **8**, 705 (2017).

[15] T. T. Tran, C. Elbadawi, D. Totonjian, C. J. Lobo, G. Grosso, H. Moon, D. R. Englund, M. J. Ford, I. Aharonovich, and M. Toth, ACS Nano **10**, 7331 (2016).

[16] X. Li, G. D. Shepard, A. Cupo, N. Camporeale, K. Shayan, Y. Luo, V. Meunier, and S. Strauf, ACS Nano **11**, 6652 (2017).

[17] N. R. Jungwirth, B. Calderon, Y. Ji, M. G. Spencer, M. E. Flatté, and G. D. Fuchs, Nano Lett. **16**, 6052 (2016).

[18] N. Chejanovsky, M. Rezai, F. Paolucci, Y. Kim, T. Rendler, W. Rouabeh, F. Fávaro de Oliveira, P. Herlinger, A. Denisenko, S. Yang, I. Gerhardt, A. Finkler, J. H. Smet, and J. Wrachtrup, Nano Lett. **16**, 7037 (2016).

[19] A. L. Exarhos, D. A. Hopper, R. R. Grote, A. Alkauskas, and L. C. Bassett, ACS Nano **11**, 3328 (2017).

[20] N. R. Jungwirth and G. D. Fuchs, Phys. Rev. Lett. **119**, 057401 (2017).

[21] T. T. Tran, M. Kianinia, M. Nguyen, S. Kim, Z.-Q. Xu, A. Kubanek, M. Toth, and I. Aharonovich, ACS Photonics **5**, 295 (2018).

[22] B. Sontheimer, M. Braun, N. Nikolay, N. Sadzak, I. Aharonovich, and O. Benson, Phys. Rev. B **96**, 121202 (2017).

[23] T. T. Tran, C. Zachreson, A. M. Berhane, K. Bray, R. G. Sandstrom, L. H. Li, T. Taniguchi, K. Watanabe, I. Aharonovich, and M. Toth, Phys. Rev. Appl. **5**, 034005 (2016).

[24] R. Bourrellier, S. Meuret, A. Tararan, O. Stéphan, M. Kociak, L. H. G. Tizei, and A. Zobelli, Nano Lett. **16**, 4317 (2016).

[25] S. A. Tawfik, S. Ali, M. Fronzi, M. Kianinia, T. T. Tran, C. Stampfl, I. Aharonovich, M. Toth, and M. J. Ford, Nanoscale **9**, 13575 (2017).

[26] M. Abdi, J.-P. Chou, A. Gali, and M. B. Plenio, ACS Photonics **5**, 1967 (2018).

[27] N. Mendelson, Z.-Q. Xu, T. T. Tran, M. Kianinia, C. Bradac, J. Scott, M. Nguyen, J. Bishop, J. Froch, B. Regan, I. Aharonovich, and M. Toth, arXiv:1806.01199.

[28] M. Abdi, M.-J. Hwang, M. Aghtar, and M. B. Plenio, Phys. Rev. Lett. **119**, 233602 (2017).

[29] A. G. F. Garcia, M. Neumann, F. Amet, J. R. Williams, K. Watanabe, T. Taniguchi, and D. Goldhaber-Gordon, Nano Lett. **12**, 4449 (2012).

[30] J. Wolters, N. Sadzak, A. W. Schell, T. Schröder, and O. Benson, Phys. Rev. Lett. **110**, 027401 (2013).

[31] M. Pelton, Nat. Photonics **9**, 427 (2015).

[32] G. Kern, G. Kresse, and J. Hafner, Phys. Rev. B **59**, 8551 (1999).

[33] T. Tohei, A. Kuwabara, F. Oba, and I. Tanaka, Phys. Rev. B **73**, 064304 (2006).

[34] S. Reich, A. C. Ferrari, R. Arenal, A. Loiseau, I. Bello, and J. Robertson, Phys. Rev. B **71**, 205201 (2005).

[35] D. Sánchez-Portal and E. Hernández, Phys. Rev. B **66**, 235415 (2002).

[36] See Supplemental Material at http://link.aps.org/supplemental/10.1103/PhysRevB.98.081414 for a more brief description of our evaluations and measurement methods. We focus especially on to the time-constant of the spectral diffusion and the power dependence of the lifetime.

[37] W. J. Yu, W. M. Lau, S. P. Chan, Z. F. Liu, and Q. Q. Zheng, Phys. Rev. B **67**, 014108 (2003).

[38] M. L. Goldman, A. Sipahigil, M. W. Doherty, N. Y. Yao, S. D. Bennett, M. Markham, D. J. Twitchen, N. B. Manson, A. Kubanek, and M. D. Lukin, Phys. Rev. Lett. **114**, 145502 (2015).

[39] Z. Shotan, H. Jayakumar, C. R. Considine, M. Mackoit, H. Fedder, J. Wrachtrup, A. Alkauskas, M. W. Doherty, V. M. Menon, and C. A. Meriles, ACS Photonics **3**, 2490 (2016).

[40] A. Beveratos, R. Brouri, J.-P. Poizat, and P. Grangier, arXiv:quant-ph/0010044.

[41] A. L. Exarhos, D. A. Hopper, R. N. Patel, M. W. Doherty, and L. C. Bassett, arXiv:1804.09061.

[42] J. M. Binder, A. Stark, N. Tomek, J. Scheuer, F. Frank, K. D. Jahnke, C. Müller, S. Schmitt, M. H. Metsch, T. Unden, T. Gehring, A. Huck, U. L. Andersen, L. J. Rogers, and F. Jelezko, SoftwareX **6**, 85 (2017).